

Feasibility as a moving target: Fluctuating species interactions lead to universal power law in equilibrium abundances

Cagatay Eskin, Vu Nguyen, and Dervis Can Vural*

Department of Physics and Astronomy,

University of Notre Dame,

Notre Dame, Indiana 46556, USA

(Dated: February 24, 2026)

Theoretical ecology has traditionally equated persistence with the stability of a fixed equilibrium point. Here we argue that the primary threat to ecosystem persistence need not be the loss of stability, but instead the escape of the stable equilibrium to a negative orthant. In a realistic setting, fluctuations in interactions do not merely disturb abundances about an equilibrium but can displace the equilibrium point itself. We theoretically and empirically analyze such displacements of the equilibrium point in a complex community. Theoretically, we find that light-tailed fluctuations in species interactions, no matter how small, lead to a heavy-tailed power law $P(y) = 1/y^\alpha$ for the equilibrium abundance y of a species. Remarkably, the exponent $\alpha = 2$ is a universal value independent of interaction structure, community size, and species. Empirically, our analysis of 34 species reveals a power law signal for most, with a median exponent $\alpha \sim 2.56$. Next, we derive a formula for the critical noise, σ_c , beyond which the community experiences feasibility loss “with near certainty”. We find that $\sigma_c(N) \sim N^{-1}$, implying that larger communities are significantly more fragile to noise induced feasibility loss. Lastly, we define and calculate biologically measurable analytical metrics for both global and species-specific feasibility escape rates, and implement these metrics in dynamic simulations of 98 real world mutualistic and food web networks, to successfully predict their fragility.

I. INTRODUCTION

One of the central open questions in ecology concerns whether there is a tradeoff between the complexity and long term persistence of a community [1–3]. Classic theory, following May and successors, has chosen *local stability* of an equilibrium point as a key metric of persistence [4–15]. Yet stability of abundances presumes a more basic feature, *feasibility*, namely that the fixed point is located in a positive orthant. If the abundances are attracted to a fixed point with negative values, there will be extinctions and the system cannot be said to be “stable” in the biological sense, even if it may superficially be so in the mathematical sense.

Despite this foundational importance, feasibility has been studied far less than stability [16–19]. What’s known so far is that feasibility tends to vanish under “larger” interaction strengths [16] and in networks with same-sign (mutualistic and competitive) interactions [19]. Furthermore, the shape of the feasibility domain can provide insights into species-specific feasibility [18, 20].

This study investigates the relationship between the feasibility of a community, in relation to the variability of its habitat. Environmental noise does not merely disturb abundances about a fixed equilibrium point; it alters fundamental ecological parameters that determine the position of the equilibrium point in the first place.

In this case, abundances will relax perpetually towards a moving target.

We focus here on the simplest of fluctuating ecological parameters: species interactions. Interactions vary across seasons, ontogeny, behavioral contexts, productivity regimes and climate fluctuations, presumably causing changes in both the stability and feasibility of the equilibrium [3, 21–37]. Such perturbations, if large enough, might even push an equilibrium point across the feasibility boundary. How often does a community escape feasibility? How does the “escape time” of a community or individual species scale with the interaction structure, noise structure and the complexity of the web of interactions? For what fluctuation strength or time interval does feasibility loss become near certain? What substructures of an interaction network are most fragile?

In this paper, we address the above questions by calculating the probability distribution of the equilibrium point of a community with fluctuating interactions. Remarkably, we find that no matter how small these fluctuations are, the probability of large equilibrium shifts decays as a power law. Our prediction for single species fluctuations is $P(y) \sim 1/y^\alpha$ with $\alpha = 2$.

To test our prediction, we analyze two large datasets, and detect a power law signal in abundance fluctuations, to our knowledge, for the first time in the literature. We find the corresponding exponent to mostly cluster between $\alpha = 2 - 3$ (median $\alpha = 2.56$) close to our theoretical prediction.

Next, we find that the interaction noise at which feasibility loss probability becomes near certain as it shrinks with community complexity N , but exponentially ap-

* Corresponding author: dvural@nd.edu

proaches certainty ($\sim 1 - 1/2^N$) for higher levels interaction noise. This result establishes the feasibility counterpart to the complexity stability tension pointed out by the pioneering work of May [4].

Lastly, we define and calculate two metrics for risk assessment that map directly onto independently measurable quantities: (i) a species-specific “escape rate” that ranks which species are most likely to precipitate feasibility loss, and (ii) the mean time to feasibility loss for the community.

We should emphasize that unlike many previous theoretical studies that assume a specific statistical structure for the interaction matrix, such as gaussian/random, sparse, or having a particular correlation between interaction types [4–18] (including those that focus on feasibility [16–18]) we do not make any assumptions regarding the global structure of the interaction matrix: Our results hold true for any interaction structure A_{ij} , each fluctuating by their own level of noise σ_{ij} .

Leaning on this strength, we validate our analytical predictions against stochastic simulations of 98 empirical ecological networks: 82 mutualistic networks and 16 food webs. Our analytical escape-rate rankings match that of these simulated for empirical networks very well, and our predicted time to feasibility loss, tracks persistence times with high concordance.

Testing our results on empirical networks reveal interesting scaling relationships linking richness, noise, and feasibility loss, offering a quantitative framework for assessing ecosystem fragility that complements simple eigenvalue-based stability analyses and directly informs empirical design and conservation prioritization.

II. MATERIALS AND METHODS

We start with the standard generalized Lotka-Volterra (gLV) framework

$$\frac{dn_i}{dt} = n_i \left[r_i + \sum_{j=1}^N A_{ij} n_j \right] \quad (1)$$

governing the biomass $n_i(t)$ of the i^{th} species at time t , with intrinsic growth rate r_i . The biomass conversion rate from species j to i is given by the “interaction matrix” A_{ij} . Setting the square bracket to zero yields the coexistent equilibrium condition, $\vec{n}_{\text{fixed}} = \vec{x} = -\mathbf{A}^{-1}\vec{r}$. The feasibility condition is $x_i > 0$, for all i .

Even though the A_{ij} are known to fluctuate [3, 21–37] it is also unrealistic to expect them to drift away indefinitely in Brownian fashion: The constancy of fundamental resources, combined with the optimized metabolic efficiency of organisms, restores interaction values to their canonical values [27]. Furthermore, while the physical parameters influencing A_{ij} such as temperature, pH, pressure, light exposure might change day to day, they will still be distributed around their “seasonal normals”.

As such, we will assume that A_{ij} is subject to both random and restorative forces. This kind of motion is known as an Ornstein-Uhlenbeck (OU) process [38, 39], and has been used by others to describe fluctuations in environmental parameters [40, 41]. Specifically, we assume that the interaction matrix $\mathbf{A}(t) = \mathbf{A} + \delta\mathbf{A}(t)$, deviates by its mean value \mathbf{A} according to the stochastic equation

$$d(\delta A_{ij}(t)) = -k_{ij}\delta A_{ij}(t)dt + \sqrt{D_{ij}}dW_{ij}(t) \quad (2)$$

where k_{ij} and $\sqrt{D_{ij}}$ are the restorative and random influences (analogous to a spring constant and diffusion coefficient) and dW_{ij} is an infinitesimal, uncorrelated, normally distributed kick [38, 39]. We describe the random motion of the equilibrium point $\vec{y}(t) = \vec{x} + \delta\vec{y}(t)$ by the probability distribution $h(\vec{y})$.

Over long times, the OU process leads to a Gaussian distribution of $\delta A_{ij}(t)$ with individual means $\langle \delta A_{ij} \rangle = 0$ and variances $\langle \delta A_{ij}^2 \rangle = \sigma_{ij}^2 = D_{ij}/2k_{ij}$.

Note that that this is not equivalent to the random matrix models popular in the literature, where every element is chosen from a normal distribution. In our model the matrix can have any structure A_{ij} , and the normal fluctuations occur around this particular structure. Furthermore, each element has its own σ_{ij} .

III. RESULTS

Multi-Species Equilibrium Abundance Distribution. We obtain the probability distribution of equilibrium abundances, $h(\vec{y})$, using the equilibrium condition, $\vec{y} = -[\mathbf{A} + \delta\mathbf{A}]^{-1}\vec{r}$, and the distribution of $\delta\mathbf{A}$. A tedious calculation yields (see SI.1)

$$h(\vec{y}) = C \frac{e^{-\frac{1}{2}(\kappa - \vec{\psi}^T \mathbf{\Gamma}^{-1} \vec{\psi})}}{\prod_i |y_i| \sqrt{|\mathbf{\Gamma}|}} \langle |\det[\mathbf{I} + \mathbf{\Omega}_*]| \rangle \quad (3)$$

$$\psi_{ij} = (\beta_i F_{ij}^i - \beta_j y_i F_{jj}^j / y_j), \quad \Gamma_{ij,kl} = \frac{H_{ij,kl} + H_{kl,ij}}{2}$$

$$H_{ij,kl} = F_{jl}^k \left(\delta_{ik} - 2\delta_{kj} \frac{y_i}{y_k} \right) + F_{jj}^j \delta_{jl} \frac{y_i y_k}{y_j^2}, \quad F_{ij}^m = \sum_{k=1}^N \frac{A_{ki} A_{kj}}{\sigma_{km}^2}$$

$$\kappa = \sum_{i=1}^N F_{ii}^i \beta_i^2, \quad C = |\det(\mathbf{A})|^N (2\pi)^{-N/2} / \prod_{ij} |\sigma_{ij}|$$

$$(\mathbf{\Omega}_*)_{ij} = (1 - \delta_{ij})\Omega_{ij} + \delta_{ij} \left(\beta_i - \sum_{q \neq i} \Omega_{iq} y_q / y_i \right), \quad \beta_i = \frac{x_i - y_i}{y_i}$$

where $(i, j), (k, l) \in \Lambda = \{(u, v) \in \{1, \dots, N\}^2, u \neq v\}$ and the average $\langle \dots \rangle$ is over $\mathbf{\Omega}$'s distributed (normally) as $\propto \exp[-\frac{1}{2} \sum_{(i,j),(k,l) \in \Lambda} (\Omega_{ij} - \mu_{ij}) \Gamma_{ij,kl} (\Omega_{kl} - \mu_{kl})]$, with mean $\vec{\mu} = -\mathbf{\Gamma}^{-1} \vec{\psi}$. The inverse $\mathbf{\Gamma}^{-1}$ and determinant $\det(\mathbf{\Gamma}^{-1})$ are defined as $\sum_{(k,l) \in \Lambda} \Gamma_{ij,kl} (\mathbf{\Gamma}^{-1})_{kl,mn} = \delta_{im} \delta_{jn}$ and $|\mathbf{\Gamma}^{-1}| = \det[(\mathbf{\Gamma}^{-1})_{ij,kl}]_{(i,j),(k,l) \in \Lambda}$.

Universal Power Law. The tails of $h(\vec{y})$ decay as a power law. To determine the power, we decompose the abundance vector $\vec{y} = L\hat{s}$ into its magnitude L and direction \hat{s} . Analyzing the components of the

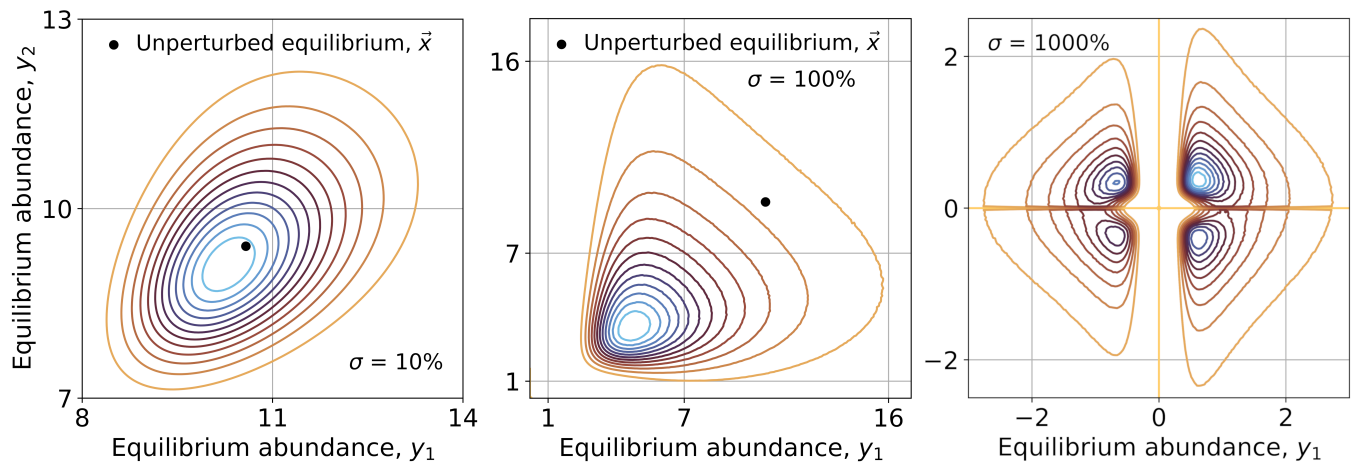


FIG. 1. **Probability distribution of equilibrium abundances for different noise levels.** We plot the exact distribution $h(\vec{y})$ for $\mathbf{A}=\{-1.4, 0.1\}, \{0.5, -1.4\}$ perturbed by 10% (left), 100% (center) and 1000% (right) noise. As the noise increases, more probability mass moves to negative quadrants, signifying increased risk. The unperturbed equilibrium is marked by \circ .

joint distribution, we observe three distinct scaling behaviors as $L \rightarrow \infty$. First, the explicit prefactor scales as $(\prod |y_i|)^{-1} \sim L^{-N}$. Second, the shape parameters (matrix Γ and exponential) depend only on equilibrium ratios and are therefore asymptotically scale-invariant ($\sim L^0$). Third, the expectation term $\langle \|I + \Omega_*\| \rangle$ scales as L^{-1} . Combining these terms, the joint distribution behaves asymptotically as a homogeneous function of degree $-(N+1)$, similar to a type-II multivariate Pareto distribution [42],

$$h(L\hat{s}) \sim K(\hat{s})L^{-(N+1)} \quad (3)$$

where $K(\hat{s})$ is a direction dependent prefactor collecting all scale invariant terms.

To obtain the marginal distribution $h(y_i)$ for a single species i , we integrate the joint distribution over the remaining $N-1$ species. We separate the magnitude of the system and its geometry to see that integration of the volume introduces a term that scales as y_i^{N-1} . Including the decay of the joint probability density ($\sim y_i^{-(N+1)}$) yields the scaling for the marginal distribution of equilibrium abundance for a single species as:

$$h(y_i) \sim 1/y_i^\alpha \quad \alpha = 2. \quad (4)$$

This power law is *universal*: It holds true for any community, and any species within, independent of the specific details of the interaction structure or strength of noise (see SI.1 for details).

The heavy tails of $h(\vec{y})$ quantify the risk of catastrophic feasibility loss. A rare but large fluctuation in the interaction matrix $\delta\mathbf{A}$ can drive the system towards a configuration where $\mathbf{A}(t)$ becomes nearly singular, causing the equilibrium \vec{y} to shift dramatically; and whichever y_i falls outside the feasible orthant, those species i are pulled towards extinction.

For visualization purposes, we pick $N=2$, and plot $h(\vec{y})$ in Fig.1 for three levels of noise. In the low noise

limit ($\sigma=10\%$), Gaussian matrix elements lead to an approximately Gaussian $h(y)$, whose peak is approximately centered around \vec{x} (Fig.1a). As the noise becomes comparable to the interaction values ($\sigma=100\%$), the distribution becomes more lopsided and the probability mass in the negative orthants start becoming comparable to that in the positive one (Fig.1b). When the noise is much larger than the interaction values ($\sigma=1000\%$), there is approximately equal probability mass across all 2^N orthants (Fig.1c).

Low-Noise Limit. If the noise perturbing the interactions is much smaller than the interactions themselves ($\|\mathbf{A}^{-1}\delta\mathbf{A}\| \ll 1$), the probability mass under the power law tail is negligible compared to that under the bulk, and $h(\vec{y})$ can be approximated by a Gaussian, whose mean $\langle \vec{y} \rangle$ and covariance $\text{Cov}(\delta y_i, \delta y_j)$ we will identify. We first expand,

$$\vec{y} = [\mathbf{A} + \delta\mathbf{A}]^{-1}\vec{r} = [\mathbf{I} + \mathbf{A}^{-1}\delta\mathbf{A}]^{-1}\vec{x} \simeq [\mathbf{I} - \mathbf{A}^{-1}\delta\mathbf{A}]\vec{x}$$

The deviations from equilibrium $\delta\vec{y} = \vec{y} - \vec{x} \simeq -\mathbf{A}^{-1}\delta\mathbf{A}\vec{x}$ gives us the covariance matrix (see SI.1)

$$\Sigma_{ij} = \text{Cov}(\delta y_i, \delta y_j) = \langle \delta y_i \cdot \delta y_j \rangle = \sum_{kl} x_k^2 \sigma_{lk}^2 A_{il}^{-1} A_{jl}^{-1}.$$

Up to first order in noise, there is no shift in the mean, $\langle \vec{y} \rangle = \vec{x}$. The shift emerges upon expanding up to second order in noise (see SI.1),

$$\langle y_i \rangle = x_i + \sum_{kj} A_{ij}^{-1} A_{kj}^{-1} \sigma_{jk}^2 x_k. \quad (5)$$

Figure 2 shows the equilibrium abundance distribution $h(\vec{y})$ for the $N=2$ case, plotted alongside the above low-noise (Gaussian) approximation. The inset shows the distribution's tails, which exhibit a power law scaling with an exponent of $N+1$ (further examples of tail scaling for different ecosystems are provided in SI.1).

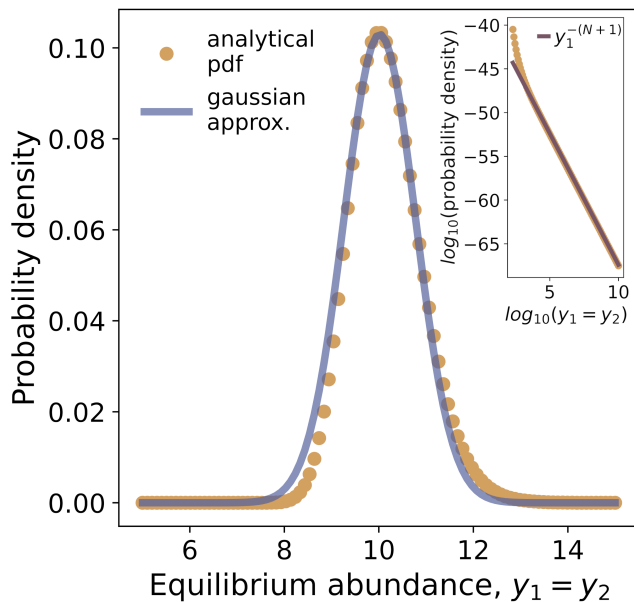


FIG. 2. **The bulk and tail behavior of $h(\vec{y})$.** As we move along the main diagonal $|y| = y_1 = y_2$ the distribution turns from a Gaussian to a power law $1/|y|^{N+1}$. The power law scaling is the same in every direction. The parameters used in the figure are same as Fig.1 with $\sigma = 8\%$.

Empirical evidence for heavy tails. We now analyze two large empirical datasets to see if abundance fluctuate according to a power law, and if so what the power α is.

The first dataset is a synthesis of 33 years of whole lake measurements, where nutrient loads and food webs in several lakes were manipulated to study ecosystem responses [43, 45]. For our purposes analysis, we focus specifically on Paul Lake, which served as the unmanipulated “control group” in [43]. The second dataset is a laboratory mesocosm containing a Baltic Sea plankton community, specifically designed to maintain strictly consistent external conditions for over 2,300 days [44].

We conduct our power law analyses by following the strict framework of [46]. Specifically, we first estimate the lower bound of the power law by minimizing the Kolmogorov-Smirnov (KS) statistic between the empirical data and the fitted power law model. Next, we evaluate the plausibility of the power law hypothesis using a goodness of fit test based on semi parametric bootstrapping. In this framework, the null hypothesis is that the data are drawn from a power law distribution; therefore, we reject the power law model if the resulting p -value is below a threshold (we pick $p \leq 0.1$, which is more cautious than the standard $p \leq 0.05$). For the remaining fits that pass the test, we employ likelihood ratio tests to compare the power law model against alternative distributions, specifically the exponential and lognormal distributions. Finally, as an additional step beyond the standard procedure, we apply the Augmented Dickey-

Fuller test to detect non stationarity in the abundance time series. We exclude datasets exhibiting significant directional trends to ensure that heavy tails arise from internal dynamics rather than external forcing.

Fig.3 shows the analysis of heavy tailed biomass fluctuations of species across two datasets. Fig.3A shows Complementary Cumulative Distribution Functions (CCDF), $P(X \geq x)$ and corresponding time series for six representative species. In the log-log CCDF (complementary cumulative distribution function) plots, the empirical data aligns closely with a heavy tailed a power law, and diverges significantly from an exponential tail. Fig.3B summarizes the distribution of the power law exponents, α , across all species where a power law model was highly plausible ($p \geq 0.1$).

The tail exponents cluster between 2 and 3, with a median value of $\alpha = 2.56$, not too far from our analytical value $\alpha_t = 2.0$ (Eqn. 4). This cluster falls under the “heavy tail regime” where the distribution does not have a finite variance despite having a finite mean.

Fig.3C shows the goodness of fit values derived from the Kolmogorov-Smirnov test, for all species from the combined datasets. The results reveal that heavy tailed distributions are a recurrent feature in these communities, irrespective of the system scale. We mark with asterisks the species for which a power law is not only plausible but statistically favored over an exponential alternative (Likelihood Ratio test, $\mathcal{R} > 0, p < 0.1$).

The likelihood ratio tests comparing the log-normal distribution against the power law did not statistically significantly favor the log-normal model over a power law characterization of the tail. This is not surprising, since our analytical form approximates to a Gaussian near the peak and transitions into a heavy tail moving out, just like a log-normal. It is well known that distinguishing between a power law and a log-normal distribution is extremely difficult and often inconclusive unless the dataset is exceptionally large [46].

In SI.1, we study how a non-linear functional response affects the power law behavior. Specifically we consider a Holling type functional response $\phi_i(n_i) = \alpha_i n_i^{m_i} / (\beta_i^{m_i} + n_i^{m_i})$, for the i^{th} species, and find that the heavy tails persist. However, in this case, the value of α depends on the power of the functional response, $\alpha = m_i + 1$. This dependence could account for some of the variation in Fig.3B and Fig 3C. Since a Holling exponent is typically between 1-3 for most species, this would also explain why the value of α is similar across so many species (Fig.2, Fig.3).

Furthermore, we show that in the low noise limit, the abundance distribution in this Holling-type response can be approximated by a log-normal distribution (SI.1). The log-normal model is marked as plausible by all 34 species we analyze, with the least plausible one having $p = 0.13$, above our conservative $p = 0.1$ threshold.

Measures of Feasibility. Now we address (i) which species are most vulnerable to feasibility loss, and (ii) what is the persistence time of feasibility. (i) and (ii)

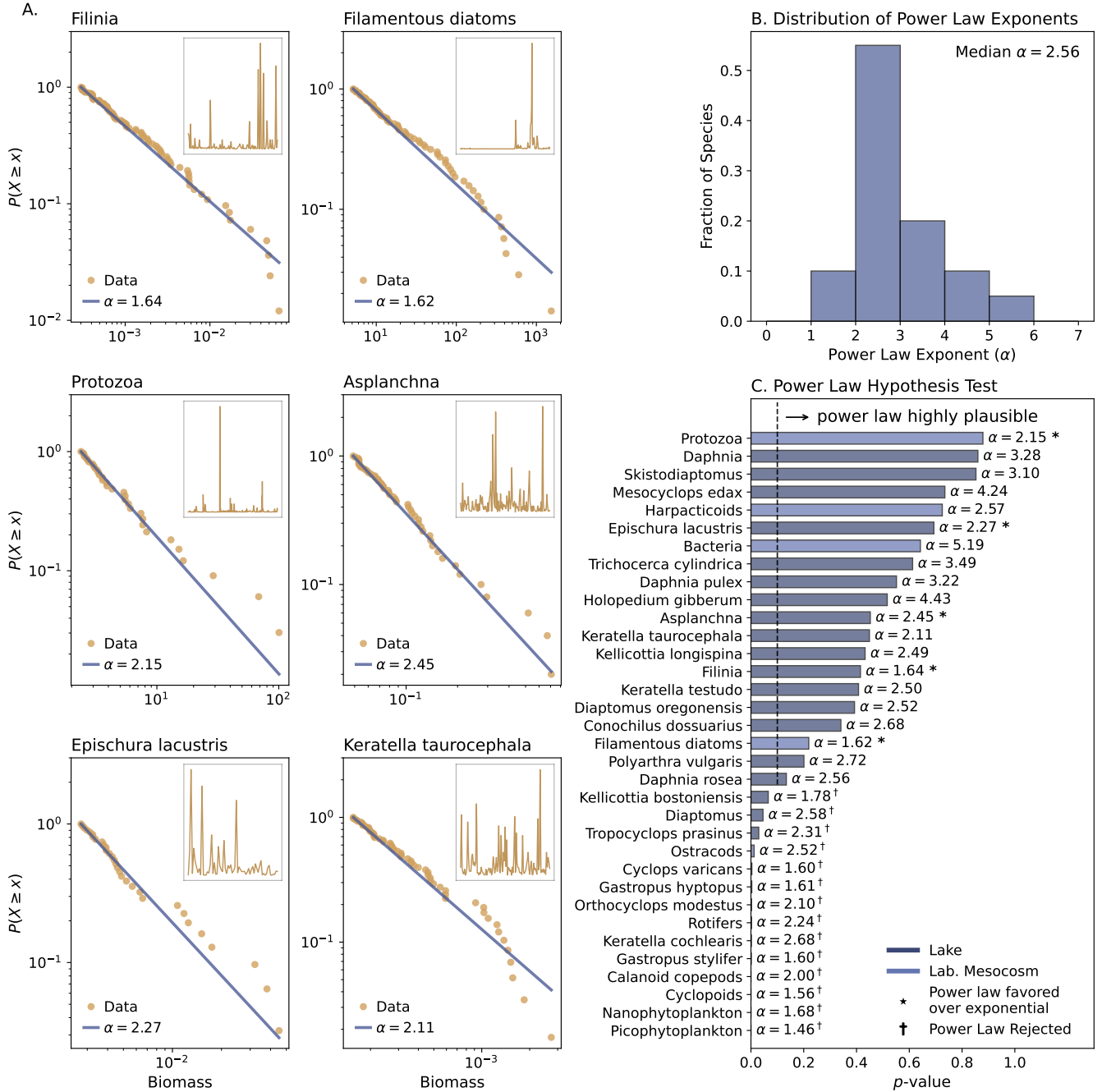


FIG. 3. Evidence of heavy tailed abundance distributions in aquatic communities (A) Complementary Cumulative Distribution Functions (CCDF) for the tails of abundance on a log-log scale. Empirical data are shown as gold circles; the solid blue line represents the best fit power law distribution ($P(X \geq x) \propto x^{-(\alpha-1)}$). In the insets of each panel abundance time series of the species/functional groups are given where units are fresh weight concentration (mg/L) for Mesocosm dataset and dry mass density for Lake dataset. [43]. (B) Stacked histogram showing the distribution of power law exponents (α) for all species identified as having plausible power law tails ($p \geq 0.1$). The data combines results from a 33 year field study of a reference lake (dark blue) [43] and a 7 year constant condition laboratory mesocosm (light blue) [44]. (C) Assessment of the power law hypothesis. Bars indicate the p -value from a Kolmogorov-Smirnov goodness of fit test using 10,000 semiparametric bootstrap simulations; values $p \geq 0.1$ indicate that the power law model cannot be rejected. Labels denote the estimated exponent (α) for each species. An asterisk (*) indicates a statistically significant preference for the power law over an exponential distribution (Likelihood Ratio Test, $\mathcal{R} > 0, p < 0.1$). In all analyses, no statistically significant preference for the log-normal distribution over the power law was found.

will constitute our local and global measures of feasibility, which we will then compare with simulations of real-life communities.

In the low noise regime we can linearize the deviation from equilibrium, $\delta\vec{y}(t) \approx -\mathbf{A}^{-1}\delta\mathbf{A}(t)\vec{x}$. Evidently, $\delta\vec{y}$ is a sum of OU processes, which in general is not an OU process itself. Nevertheless, for first-passage estimates in the low-noise regime, it is convenient to approximate δy_i by an *effective* OU process that matches the stationary variance s_i^2 and the instantaneous diffusion D_{ii}^{eff} (SI.2),

$$d(\delta y_i) \approx -\gamma_i \delta y_i dt + \sqrt{2D_{ii}^{\text{eff}}} dW_i, \quad \gamma_i = D_{ii}^{\text{eff}}/s_i^2 \quad (6)$$

$$D_{ii}^{\text{eff}} = \sum_{jk} (A_{ij}^{-1} x_k)^2 k_{jk} \sigma_{jk}^2, \quad s_i^2 = \sum_{jk} (A_{ij}^{-1} x_k)^2 \sigma_{jk}^2$$

This approximation preserves the correct Gaussian stationary variance (since $s_i^2 = D_{ii}^{\text{eff}}/\gamma_i$) and the correct short-time spreading, while compressing the multi-timescale correlation structure into a single effective relaxation rate (SI.2). The corresponding Fokker-Planck equation is [38, 39]:

$$\frac{\partial}{\partial t} p(\delta y_i, t) = \frac{\partial}{\partial \delta y_i} [\gamma_i \delta y_i p(\delta y_i, t)] + D_{ii}^{\text{eff}} \frac{\partial^2}{\partial \delta y_i^2} p(\delta y_i, t)$$

Imposing an absorbing boundary at 0 and a reflecting boundary at infinity, gives us a Kramer's formula for the extinction rate [38, 39] (SI.2):

$$\lambda_i \approx \frac{\gamma_i \chi_i}{\sqrt{2\pi}} e^{-\chi_i^2/2}, \quad \chi_i = \frac{x_i}{s_i} \quad (7)$$

The dominant parameter in Eq.7 is the barrier-to-fluctuation ratio χ_i . Species with smaller abundances with larger fluctuations carry exponentially higher risk of feasibility loss. Assuming extinction events occur independently as a Poisson processes, the system-wide mean time to feasibility loss is $\langle T_{\text{loss}} \rangle \simeq (\sum \lambda_i)^{-1}$. We identify λ_i and $\langle T_{\text{loss}} \rangle$ as a measures of individual and global robustness.

To test these predictions, we parameterize 98 empirical ecological networks from [48], consisting of 82 mutualistic networks and 16 food webs. Using these empirical structures, we generate ensembles of globally stable interaction matrices for each network, similar to [18]. For mutualistic networks, we vary the mean positive interaction strength and the coefficient of variation (CV). For food webs, we vary the ratio of negative to positive interaction strengths (μ_{ratio}) and the CV, generating four parameter sets per network type. We then compare our analytical predictions with stochastic simulations ran on these empirical network structures. The stochastic dynamics is out by numerically integrating Eqn.2 using an Euler–Maruyama scheme, with the equilibrium recalculated at each step until feasibility loss occurred.

In the top panel of Fig.4 we show the interaction structure of an example of mutualistic ecosystem of 12 seed dispersers and 7 plants measured in Spain [48, 49]. In such a mutualistic network all intergroup interactions are

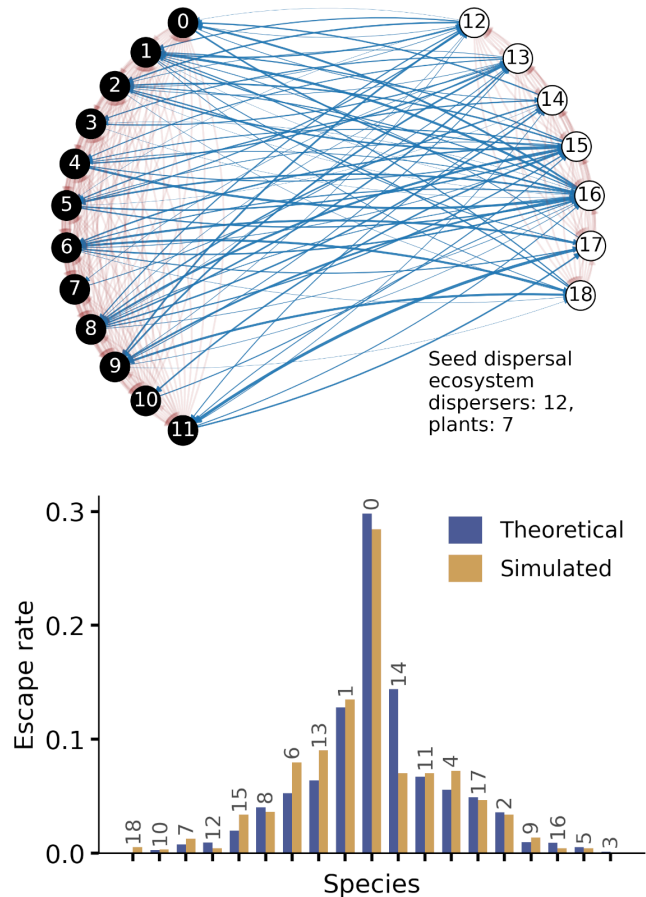


FIG. 4. **A mutualistic seed dispersal network observed in Spain [47, 48] and the risk predictions for each species.** The top panel illustrates the structure of a representative mutualistic network, composed of 12 disperser species (black nodes) and 7 plant species (white nodes). As is characteristic of this community, interactions are defined due to competition (negative, red edges) within each group and interspecific mutualism (positive, blue edges) between the two groups. The bottom panel directly compares our analytical predictions with simulation results. It shows the normalized escape rate for each species, calculated from Eq.7, alongside the corresponding feasibility loss ratios from stochastic simulations. The results demonstrate a strong correspondence, with the species predicted to have the highest escape rate also accounting for approximately one third of all simulated feasibility loss events. This predictive power, which also captures both the ranked importance and the relative contribution of each species to community fragility is a good example of predictive power of derived escape rate formula Eqn. 7.

sampled from a positive average that guarantees global stability of the initial system. On the contrary, intra-group interactions are sampled from a negative average value to stand for competition. Fig.4 (bottom) shows our normalized escape rate predictions (Eqn. 7) and corresponding feasibility loss rates from simulations. We find good agreement for both the rank order and numerical

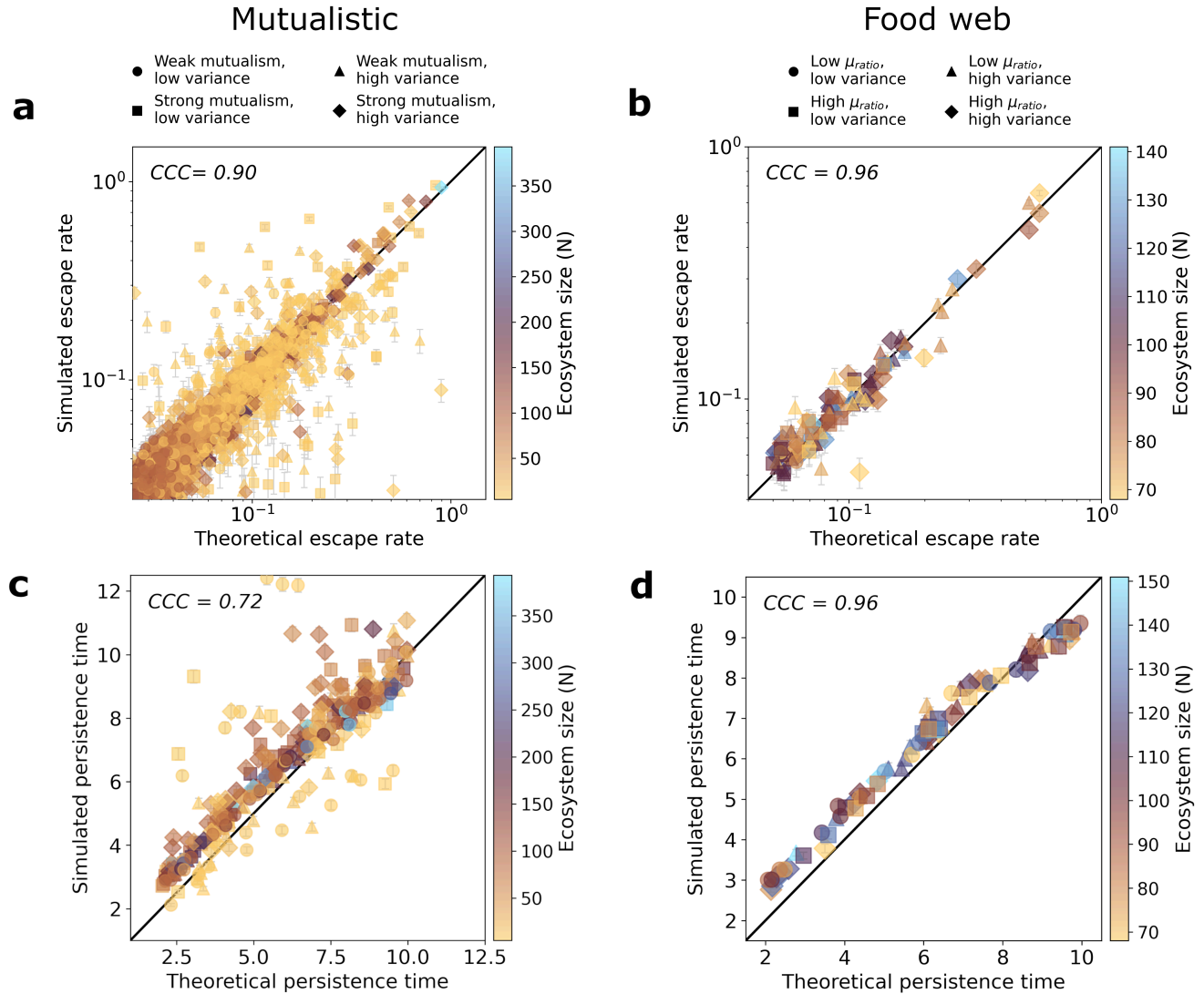


FIG. 5. **Feasibility loss rate and mean time to loss for empirical networks alongside analytical predictions.** Each panel compares an analytical prediction (x-axis) against results from stochastic Monte Carlo simulations (y-axis), with the solid black line representing the line of perfect agreement. (a, b) The relationship between the analytical escape rate ratio (normalized Eqn. 7) and the simulated corresponding loss probability. Each point corresponds to a single species within an ecosystem. Larger escape rate values indicate that the ecosystem is more likely to lose feasibility through that species, signifying its higher fragility. Panel (a) shows results for mutualistic networks, and (b) shows results for food webs. (c, d) The relationship between analytical and simulated mean time to feasibility loss. Each point represents an entire ecosystem, calculated as the inverse of the total escape rate. A larger persistence time indicates greater ecosystem robustness against fluctuations. Panel (c) shows results for mutualistic networks, and (d) shows results for food webs. For all panels, the color of each point corresponds to the size of the ecosystem (S), as indicated by the color bars. Marker shapes describe how the network is parameterized: for mutualistic networks, they distinguish between weak and strong mutualism and low and high variance (CV). For food webs, markers distinguish between a low and high ratio of negative to positive interaction, μ_{ratio} and low and high variance (CV). The model shows substantial agreement for food webs (Concordance Correlation Coefficient, $CCC = 0.96$ for both metrics), while showing moderate agreement for the mutualistic networks ($CCC = 0.72$ for persistence time, $CCC = 0.90$ for escape rates). For the panels (a) and (b) we excluded the species with escape rate or corresponding loss ratio values below 0.05. For each of the parametrized networks we ensured the starting system is globally stable and feasible. For panels (a) and (d) weak mutualism corresponds to average positive interaction value $0.2 \times \mu_{max}$ where μ_{max} is maximum allowed average of positive interactions to ensure global stability. Similarly for strong mutualism this value is $0.6 \times \mu_{max}$. For all the panels, low variance and high variance correspond to $CV = 0.5$ and $CV = 2.0$, respectively. Also, negative in-group interactions representing competition are taken as 0.25 for all the panels.

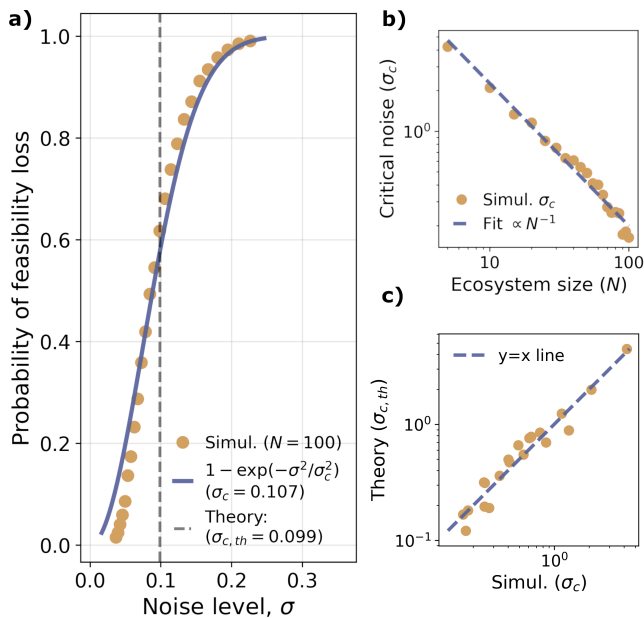


FIG. 6. **Analysis of probability of feasibility loss for random networks.** We consider May type fully connected interaction matrices with Gaussian distributed elements to simulate the change of probability of feasibility loss with the increasing noise variance. We observe that the loss probability fits an exponential saturation model with a decay rate σ_c^2 after which feasibility loss is almost certain. Repeating the simulations for different ecosystem sizes we observe that the critical noise, σ_c scales with ecosystem size as a power law with exponent -1 . Panel a) shows the probability of feasibility loss obtained through Monte Carlo simulations as a function of the noise level for a $N = 100$ system. The panel b) shows the result of simulations for different ecosystems with increasing number of species and their respective σ_c fit values. We observe that as the ecosystem size increases, critical noise level which leads to almost certain feasibility loss decays with the power law $\propto N^{-1}$. Panel c) shows the difference between σ_c obtained by fitting the simulation results versus theoretical prediction Eqn. 8.

values of feasibility loss risk.

The broader analysis across all networks is summarized in Fig.5. For food webs, the analytical model strongly predicts both escape rates and feasibility persistence times (Concordance Correlation Coefficient, CCC = 0.96 for both metrics). For mutualistic networks, agreement is also substantial (CCC = 0.72 for persistence times and CCC = 0.90 for escape rates).

Conditions for Almost Certain Feasibility Loss

In the high noise regime ($\delta A_{ij} \gg A_{ij}$), significant probability mass leaks out of the all positive orthant as $h(\vec{y})$ uniformizes across all 2^N orthants, therefore the probability of feasibility loss approaches $1 - 1/2^N$ (Fig.6), and accordingly, the mean time to feasibility

loss approaches 0. In Fig.6 we numerically simulate $\vec{y}(t) = -[\mathbf{A} + \delta\mathbf{A}(t)]^{-1}\vec{r}$ to show how quickly feasibility loss converges to these asymptotes with increased noise ($\sigma^2 = D/2k$) for various community sizes N . Feasibility loss probability is best fit by exponential saturation (Fig.6 left). Specifically, as noise is increased, the system converges to “certain infeasibility” at a rate of σ_c^2 . We find that larger communities are more sensitive to noise; specifically, $\sigma_c \sim 1/N$. As $N \rightarrow \infty$, an infinitesimal noise $\sigma \rightarrow 0$ leads to feasibility loss with near certainty.

In the opposite limit of low noise ($\delta A_{ij} \ll A_{ij}$), feasibility can still be lost with very high probability. We have shown earlier that in the low noise limit $h(\vec{y})$ is approximately a Gaussian, peaked around the shifted equilibrium with components $\langle y_i \rangle = x_i + \sum_{kj} A_{ij}^{-1} A_{kj}^{-1} \sigma_{jk}^2 x_k$ where \vec{x} is the unperturbed equilibrium. With increasing noise, the distribution broadens significantly faster than the mean shifts. A rough estimate for what amount of noise will cause almost certain feasibility loss can be obtained considering the broadening of the distribution and setting $\text{Var}(y_i) = \langle y_i \rangle^2$, and $\sigma_i \sim \sigma$ in Eqn.5,

$$\sigma_{c,th} = \frac{\langle y_i \rangle}{\sqrt{\sum_{kl} (A_{il}^{-1})^2 \langle y_k \rangle^2}} \quad (8)$$

This estimate is marked in Fig.6, Panel a) with the dashed line and agrees well with the value σ_c marking the transition to certain feasibility loss. Panel b) shows the scaling of critical variance with increasing ecosystem size obtained through the simulations and the Panel c) shows difference between σ_c obtained from the simulations and theoretical prediction, $\sigma_{c,th}$.

IV. DISCUSSION

Our results present a feasibility centered perspective on the complexity–persistence debate. When interactions fluctuate, the equilibrium is no longer a fixed point but a stochastic, moving target; consequently, persistence can fail even when the instantaneous dynamics remain stable.

We have come to the startling conclusion that light-tailed (Gaussian) perturbations to interaction values, no matter how small, will lead to heavy tailed equilibrium distributions. Moreover, this result is quantitatively universal: the power law $h(y) \sim 1/y^2$ does not depend on community size and interaction structure.

To quantify the strength of feasibility, we introduced two biologically interpretable, empirically measurable metrics (cf. Eqn.7 and paragraph below). These metrics translate interaction statistics into a ranking of species vulnerability and global feasibility.

Our analysis of empirical data reveals a recurrent power law scaling with an exponent mostly clustered within $\alpha \sim 2 - 3$ (median $\alpha = 2.56$), placing real world ecosystems within a heavy-tailed regime. Empirical estimates are consistent with the theoretical scaling prediction $\alpha = 2$. However, this raises the question of why the

theory systematically underestimates the exponent, and why a finite variance in α across species exist in the first place, despite our finding that α is not structure, size, and species dependent.

First, our analysis in S.I. shows that modifying the simple Lotka-Volterra functional response to a Holling-Type functional response, turns the $h(y) \sim 1/y^2$ law into $h(y) \sim 1/y^{m+1}$, where m is the Holling exponent. This explains not only the finite species to species variability in Fig.3, but also why the variability remains limited: In nature, m tends to range between 1-3 (corresponding to an apparent $\alpha = 2 - 4$), successfully accounting for most of the variability in our α data.

Second, we should remind and caution that we use empirical abundance values $n(t)$ as a proxy for equilibrium values $y(t)$. This is fair for species whose relaxation times are faster than the random motions of interactions. But slow-relaxing species will never have time to catch up with the equilibrium, on the rare occasion that it jumps to some far extreme. This effectively shaves off the extremes, increasing the apparent value of α . If the effect is sufficiently large, it could even wash away the power law signal below our significance threshold. The variation in relaxation times of different species then, would cause a spread in α values, while also pushing them ahead.

Our findings have critical implications for how we understand ecological risk and connects directly to the literature on the theory of community persistence. We suggest that the primary threat to a community's persistence may not be the failure of local stability, but rather a sudden, fluctuation driven shift of the entire equilibrium into

an unfeasible state. This might provide a mechanism for the black swan events where a community that appears robust and stable for long periods can, nevertheless, suddenly crash [50]. As such, merely observing the stability of population dynamics around a mean value seems insufficient. One must account for the inherent risk of large, intermittent shifts in the equilibrium value itself.

Feasibility loss constitutes an additional fragility channel to May's eigenvalue stability: The larger a community, the more easily its equilibrium point can be pushed into infeasibility, even though the equilibrium point itself can maintain its stability at all times.

DATA AVAILABILITY

Time series abundance data for the whole lake experiments were acquired from the BioTIME database (dataset 638) and [43, 45]. Data for the laboratory mesocosm experiment were obtained from [44]. The interaction networks used for the feasibility analysis of 98 empirical ecosystems were retrieved from the Web of Life repository [48, 49]. The source codes necessary to reproduce all the results are available in the GitHub repository github.com/cagatayeskin/Feasibility_analysis.

ACKNOWLEDGMENTS

We thank Notre Dame Center for Research Computing for allowing us to utilize their computational sources during the production of this paper.

-
- [1] S. L. Pimm, *Nature* **307**, 321 (1984), publisher: Nature Publishing Group.
 - [2] A. R. Ives and S. R. Carpenter, *Science* **317**, 58 (2007), publisher: American Association for the Advancement of Science.
 - [3] S. Allesina and S. Tang, *Nature* **483**, 205 (2012), publisher: Nature Publishing Group.
 - [4] R. M. May, *Nature* **238**, 413 (1972).
 - [5] R. M. May, *Stability and Complexity in Model Ecosystems* (Princeton University Press, Princeton, NJ, 1973).
 - [6] F. de Castro, S. M. Adl, S. Allesina, R. D. Bardgett, T. Bolger, J. J. Dalzell, M. Emmerson, T. Fleming, D. Garlaschelli, J. Grilli, S. E. Hannula, F. de Vries, A. G. Maule, D. H. Wall, T. Caruso, and Z. Lindo, *Ecology and Evolution* **11**, 16070 (2021).
 - [7] L. Stone, *Marine Ecology Progress Series* **64**, 137 (1990).
 - [8] S. Rao, N. Muyinda, and B. De Baets, *Scientific Reports* **11**, 1 (2021).
 - [9] X. Chen and J. E. Cohen, *Journal of Theoretical Biology* **212**, 223 (2001).
 - [10] X.-Z. He, S. Ruan, and H. Xia, *SIAM Journal on Mathematical Analysis* **29**, 681 (1998).
 - [11] S. H. Roxburgh and J. B. Wilson, *Oikos* **88**, 395 (2000).
 - [12] G. Gellner, K. McCann, and A. Hastings, *Proceedings of the National Academy of Sciences* **120**, e2212061120 (2023).
 - [13] U. Brose, R. J. Williams, and N. D. Martinez, *Ecology Letters* **9**, 1228 (2006).
 - [14] J. Grilli, T. Rogers, and S. Allesina, *Nature Communications* **7**, 12031 (2016), publisher: Nature Publishing Group.
 - [15] C. A. Serván, J. A. Capitán, J. Grilli, K. E. Morrison, and S. Allesina, *Nature Ecology & Evolution* **2**, 1237 (2018), publisher: Nature Publishing Group.
 - [16] M. Dougoud, L. Vinckenbosch, R. P. Rohr, L.-F. Bersier, and C. Mazza, *PLOS Computational Biology* **14**, e1005988 (2018), publisher: Public Library of Science.
 - [17] S. Saavedra, R. P. Rohr, J. Bascompte, O. Godoy, N. J. B. Kraft, and J. M. Levine, *Ecological Monographs* **87**, 470 (2017).
 - [18] J. Grilli, M. Adorisio, S. Suweis, G. Barabás, J. R. Banavar, S. Allesina, and A. Maritan, *Nature Communications* **8**, 14389 (2017), publisher: Nature Publishing Group.
 - [19] X. Liu, G. W. A. Constable, and J. W. Pitchford, *Physical Review E* **107**, 054301 (2023), publisher: American Physical Society.
 - [20] A. Allen-Perkins, D. García-Callejas, I. Bartomeus, and O. Godoy, *Ecology Letters* **26**, 1647 (2023).
 - [21] E. R. Deyle, R. M. May, S. B. Munch, and G. Sugihara, *Proceedings of the Royal Society B: Biological Sciences*

- 283**, 20152258 (2016), publisher: Royal Society.
- [22] M. Ushio, C.-h. Hsieh, R. Masuda, E. R. Deyle, H. Ye, C.-W. Chang, G. Sugihara, and M. Kondoh, *Nature* **554**, 360 (2018).
- [23] G. Sugihara, R. May, H. Ye, C.-h. Hsieh, E. Deyle, M. Fogarty, and S. Munch, *Science (American Association for the Advancement of Science)* **338**, 496 (2012).
- [24] J. T. Wootton and M. Emmerson, *Annual Review of Ecology, Evolution, and Systematics* **36**, 419 (2005), publisher: Annual Reviews.
- [25] E. L. Berlow, A.-M. Neutel, J. E. Cohen, P. C. De Ruiter, B. Ebenman, M. Emmerson, J. W. Fox, V. A. A. Jansen, J. Iwan Jones, G. D. Kokkoris, D. O. Logofet, A. J. McKane, J. M. Montoya, and O. Petchey, *Journal of Animal Ecology* **73**, 585 (2004).
- [26] W. W. Murdoch, *Ecological Monographs* **39**, 335 (1969), publisher: Ecological Society of America.
- [27] L. Oksanen, S. D. Fretwell, J. Arruda, and P. Niemel, *The American Naturalist* **118**, 240 (1981), publisher: [The University of Chicago Press, The American Society of Naturalists].
- [28] E. E. Werner and J. F. Gilliam, *Annual review of ecology and systematics* **15**, 393 (1984).
- [29] S. L. Lima and L. M. Dill, *Canadian Journal of Zoology* **68**, 619 (1990).
- [30] E. L. Preisser, D. I. Bolnick, and M. E. Benard, *Ecology* **86**, 501 (2005), publisher: Ecological Society of America.
- [31] M. E. Visser and C. Both, *Proceedings of the Royal Society B: Biological Sciences* **272**, 2561 (2005), publisher: Royal Society.
- [32] L. H. Yang, J. L. Bastow, K. O. Spence, and A. N. Wright, *Ecology* **89**, 621 (2008), publisher: Ecological Society of America.
- [33] C. Ratzke, J. Barrere, and J. Gore, *Nature Ecology & Evolution* **4**, 376 (2020), publisher: Nature Publishing Group.
- [34] N. C. Stenseth, G. Ottersen, J. W. Hurrell, A. Mysterud, M. Lima, K.-S. Chan, N. G. Yoccoz, and B. Ådlandsvik, *Proceedings of the Royal Society. B, Biological sciences* **270**, 2087 (2003).
- [35] J. H. Brown, J. F. Gillooly, A. P. Allen, V. M. Savage, and G. B. West, *Ecology* **85**, 1771 (2004), publisher: Ecological Society of America.
- [36] S. Allesina and S. Tang, *Population Ecology* **57**, 63 (2015).
- [37] G. Barabás, M. J. Michalska-Smith, and S. Allesina, *Nature Ecology & Evolution* **1**, 1870 (2017), publisher: Nature Publishing Group.
- [38] K. Jacobs, *Stochastic processes for physicists: understanding noisy systems* (Cambridge University Press, 2010).
- [39] C. W. Gardiner, *Stochastic Methods : A Handbook for the Natural and Social Sciences*, 4th ed., Springer Series in Synergetics ; 13 (Springer Berlin, Berlin, 2010).
- [40] J. Ripa and P. Lundberg, *Proceedings of the Royal Society. B, Biological sciences* **263**, 1751 (1996).
- [41] R. Lande, S. Engen, and B.-E. Sæther, *Stochastic population dynamics in ecology and conservation*, Oxford Series in Ecology and Evolution (Oxford University Press, New York, 2003).
- [42] S. Kotz, *Continuous multivariate distributions*, 2nd ed., Wiley series in probability and statistics (Wiley, New York, 2000).
- [43] S. R. Carpenter and M. L. Pace, *Limnology and Oceanography Letters* **3**, 419 (2018).
- [44] E. Benincà, J. Huisman, R. Heerkloss, K. D. Jöhnk, P. Branco, E. H. Van Nes, M. Scheffer, and S. P. Ellner, *Nature* **451**, 822 (2008).
- [45] M. Dornelas *et al.*, *Global Ecology and Biogeography* **34**, e70003 (2025).
- [46] A. Clauset, C. R. Shalizi, and M. E. J. Newman, *SIAM Review* **51**, 661 (2009).
- [47] J. Guitián, Univ. Santiago, Spain (1983).
- [48] “Web of life: Ecological networks database,” <https://www.web-of-life.es>.
- [49] M. A. Fortuna, R. Ortega, and J. Bascompte, “The web of life,” (2014), arXiv:1403.2575 [q-bio.PE].
- [50] S. C. Anderson, T. A. Branch, A. B. Cooper, and N. K. Dulvy, *Proceedings of the National Academy of Sciences* **114**, 3252 (2017), publisher: Proceedings of the National Academy of Sciences.